JBC Papers in Press. Published on August 11, 2003 as Manuscript M306251200

Effects of Hydrogen Peroxide upon Nicotinamide Nucleotide Metabolism in *Escherichia coli*: Changes in Enzyme Levels and Nicotinamide Nucleotide Pools and Studies of the Oxidation of NAD(P)H by Fe(III)

Julia L. Brumaghim,[1] Ying Li,[2] Ernst Henle,[3] and Stuart Linn[*]

Division of Biochemistry and Molecular Biology, Barker Hall, University of California, Berkeley, CA 94720-3202, USA

Running title: *E. coli* Responses to Hydrogen Peroxide

*To whom correspondence should be addressed: Division of Biochemistry and Molecular Biology, Barker Hall, University of California, Berkeley, CA 94720-3202, USA. Tel.: 510-642-7583; Fax: 510-643-3388; E-mail: slinn@socrates.berkeley.edu

Present addresses:

[1]J. L. B.: Department of Chemistry, Clemson University, 481 Hunter Laboratories, Clemson University, Clemson, SC 29634

[2]Y. L.: Pfizer, Inc., 4125 Sorrento Valley Blvd., San Diego, CA 92121, USA

[3]E. H.: Scimagix, Inc., 2855 Campus Drive, Suite 100, San Mateo, CA 94403, USA

SUMMARY

DNA is damaged *in vivo* by the Fenton reaction mediated by Fe^{2+} and cellular reductants such as NADH which reduce Fe^{3+} to Fe^{2+} and allow the recycling of iron. To study the response of *Escherichia coli* to such cycling, the activities of several enzymes involved in nicotinamide nucleotide metabolism were measured following an H_2O_2 challenge. NADPH-dependent peroxidase, NADH/$NADP^+$ transhydrogenase, and glucose-6-phosphate dehydrogenase were most strongly induced, increasing 2.5- to 3-fold. In addition, the cellular ratios of NADPH to NADH increased 6- or 92-fold 15 min after exposure to 0.5 or 5 mM H_2O_2, respectively. *In vitro,* NADH was oxidized by Fe^{3+} up to 16-fold faster than NADPH, despite their identical reduction potentials. To understand this rate difference, the interactions of Fe^{3+} and Ga^{3+} with NAD(P)H were examined by ^1H, ^{13}C, and ^{31}P NMR spectroscopy. Association with NADH occurred primarily with adenine at N7 and the amino group, but for NADPH, strong metal interactions also occurred at the 2'-phosphate group. Interaction of M^{3+} with the adenine ring would bring it into close proximity to the redox-active nicotinamide ring in the folded form of NAD(P)H, but interaction of M^{3+} with the 2'-phosphate group would avoid this close contact. In addition, as determined by absorbance spectroscopy, the energy of the charge-transfer species was significantly higher for the Fe^{3+}/NADPH complex than for the Fe^{3+}/NADH complex. We therefore suggest that upon exposure to H_2O_2 the NADH pool is depleted and NADPH, which is less reactive with Fe^{3+}, functions as the major nicotinamide nucleotide reductant.

INTRODUCTION

The utilization of oxygen as the terminal electron acceptor for aerobic respiration results in exposure to toxic reactive oxygen species that arise as incompletely-reduced byproducts of respiratory electron transport (1) or as side products of enzymes such as xanthine oxidase, NADH/NADPH oxidase, monoxygenases, and cyclooxygenases (2,3). In addition, environmental agents such as ionizing or near-UV radiation (4) and chemicals such as paraquat, plumbagin, and menadione can generate $O_2^{\bullet -}$ and H_2O_2 in the cell (5). Reactive oxygen species cause damage to DNA, proteins, and lipids, and are implicated in a variety of human pathologies including Alzheimer's disease, cancer, arteriosclerosis, and aging (6-9).

Exposure of *E. coli* or mammalian cells to hydrogen peroxide results in two modes of killing: Mode I cytotoxicity peaks at < 3 mM H_2O_2, whereas Mode II cytotoxicity occurs between 3 and 25 mM and is independent of the dose. These complex kinetics are also observed for DNA damage *in vitro*. This toxicity is attributable to DNA damage by reactive oxygen species generated *via* the Fenton reaction (10):

$$H_2O_2 + Fe^{2+} + H^+ \dashrightarrow Fe^{3+} + [^{\bullet}OH] + H_2O.$$

The hydroxyl radical is an extremely powerful oxidant that reacts with most organic substrates at nearly diffusion-limited rates (11). Studies of oxidative DNA damage by the Fenton reaction have indicated that the species [$^{\bullet}$OH] is not free hydroxyl radical, but is likely stabilized by coordination to the DNA-bound iron (12,13).

To continue DNA damage, a reductant must be present *in vivo* to regenerate Fe^{2+} from Fe^{3+}. Genetic studies suggested that NADH might act as this reductant, and biochemical studies showed that NADH could drive DNA damage by iron and peroxide *in vivo* (10,14). The level of NAD(H) drops severely in glucose-starved *E. coli* cells, and these cells are remarkably resistant

to H_2O_2 (14). Alternatively, raising the NADH level *in vivo* by eliminating or negatively regulating NADH dehydrogenase activity either genetically or chemically by inhibiting electron transport with KCN, dramatically sensitizes *E. coli* to killing by H_2O_2. KCN does not further enhance the sensitivity of an NADH dehydrogenase mutant to H_2O_2 (14). Acceleration of DNA damage in isolated nuclei also increases dramatically in the presence of NAD(P)H and Fe^{3+} bound to EDTA or DTPA (15).

NADPH is an essential cofactor for the catalytic activities of glutathione peroxidase (16,17), catalase (18), and NADPH-dependent alkyl hydroperoxidase (19). Moreover, the majority of NADPH in mammalian cells is bound to catalase which it reactivates after the enzyme is inactivated by H_2O_2 (18,20). It might be expected that, besides NAD(P)H, glutathione could facilitate redox cycling for the Fenton reaction. However, glutathione synthase and glutathione reductase mutants exhibit normal sensitivity to Mode I killing (21,22). As a result of the induction of the *soxRS* regulon under oxidative stress, the expression of glucose-6-phosphate dehydrogenase (G6PD) increases, resulting in the conversion of $NADP^+$ to NADPH and making these cells resistant to oxidants (23,24). While it was initially believed that reduced glutathione was responsible for the antioxidant effects of the *soxRS* response, it was shown that the redox state of NADPH, not glutathione, modulates oxidative sensitivity (25). This antioxidant role of G6PD was further substantiated by observations that disruption of the gene encoding G6PD in mouse embryonic stem cells resulted in greatly enhanced sensitivity to oxidative stresses (26). and that *S. cerevisiae G6PD* null mutants also are sensitive and unable to adapt to hydrogen peroxide (27,28). The introduction of an intracellular NADPH-generating system restored substantial oxidative stress resistance to the G6PD-deficient yeast (25). In sum, NADPH is clearly important for protection against oxidative stress (26).

In order to better understand the role of NADPH in resistance to oxidative stress, the effects of H_2O_2 on the activities of several enzymes involved in the synthesis and utilization of NAD(P)H and changes in the nicotinamide nucleotide pools have been monitored following exposure of *E. coli* to H_2O_2. In addition, the relative abilities of NADH and NADPH to reduce Fe^{3+} to Fe^{2+}, as well as the nature of Fe^{3+} interactions with NAD(P)H, were studied.

EXPERIMENTAL PROCEDURES

Bacterial Strains, Buffers, and Reagents - *E. coli* strains AB1157 (*F- thr-1 leuB proA2 his-4 thi-1 argE2 lacY1 galK2 rpsL supE*) and UM1 (*LacY rpsL thi-1 katE1 katG14*) were grown with vigorous shaking in K medium (1% glucose, 1% Casamino acids, 1 mM $MgSO_4$, 0.1 mM $CaCl_2$, and M9 salts) unless otherwise noted. Water was double-distilled before use. H_2O_2 (30%) was from Fisher Scientific, NADH (disodium salt), NADPH (tetrasodium salt), and NMNH (disodium salt) were from Sigma-Aldrich. All other chemicals were from Sigma-Aldrich unless otherwise specified. Solutions of Fe^{3+} and Ga^{3+} salts were freshly prepared prior to use and stored at pH 2.5. Elemental analyses were performed by Desert Analytics (Tucson, AZ).

Spectroscopic Measurements - ^{1}H, $^{13}C\{^{1}H\}$, and $^{31}P\{^{1}H\}$ NMR spectra were acquired on a Bruker DRX-500 spectrometer at 500, 125, and 202 MHz, respectively. Chemical shifts for ^{1}H, $^{13}C\{^{1}H\}$ and $^{31}P\{^{1}H\}$ NMR spectra are reported in ppm (δ) relative to $SiMe_4$ and 40% H_3PO_4, respectively. Absorbance spectra for NAD(P)H were acquired on a Hewlett-Packard 8453 spectrophotometer with a diode array detector or a Cary 300 dual beam spectrophotometer. Kinetics measurements of NAD(P)H oxidation utilized the Cary spectrophotometer.

Chromatography – Nicotinamide nucleotides were resolved on a Perkin Elmer 250 HPLC apparatus equipped with a guard column and a Jordi reverse phase C18-DVB column (250 mm length × 4.6 mm ID). The mobile phase was 98% 25 mM tributylammonium bicarbonate (pH 10), 2% acetonitrile (eluent A) and 80% acetonitrile, 20% water (eluent B). A gradient program was initially set to 100% eluent A, increasing over 20 min to 65% eluent A and 35% eluent B, then finally increasing over 40 min to 50% each of eluents A and B. Absorbances of the nucleotides were monitored at 327 nm with a diode array detector.

Enzyme Assays - *E. coli* cells in K medium were challenged with 50 μM H_20_2 at a density of 4 × 10^7 cells/ml. After 15 min at 37 °C, the bacteria were chilled, washed and harvested by centrifugation. Cell pellets were resuspended in 5 ml of 50 mM KCl, 5 mM DTT, 100 mM Tris-HCl, pH 8.0, and the suspensions were sonicated four times for 15 s and then cleared by centrifugation. Protein concentration was determined by the method of Bradford (29).

NAD^+ kinase activity was assayed by a procedure similar to that of Zercz *et al*. (30), but [^{32}P]NAD^+ was the substrate and $NADP^+$ was monitored by radioactivity after isolation with thin layer chromatography on silica plates with ethanol : 1 M ammonium acetate (1:1) as solvent. Glucose-6-phosphate dehydrogenase and isocitrate dehydrogenase activities were assayed according to the protocols described in the Worthington manual (31). The assay of NADH transhydrogenase activity was based on the method of Zercz *et al*. (30). NADH dehydrogenase and NAD(P)H oxidases were assayed as described by Cavari *et al*. (32). NAD(P)H-dependent peroxidases were partially purified by ammonium sulfate fractionation and DEAE-cellulose chromatography and assayed following the method of Coves *et al*. (33). The reaction was carried out under aerobic conditions and in the presence of an NADH-generating system. The activity was determined from the appearance of absorbance of NADPH at 340 nm. NAD^+ pyrophosphatase activity was determined as described previously (34). The assay of DNA ligase activity was based on the method of Olivera *et al*. (35), and NAD^+ glycohydrolase assays were based on the method of Barbieri *et al*. (36).

Measurement of E. coli *Nicotinamide Nucleotide Pools* - Intracellular NAD(P)H and $NAD(P)^+$ concentrations were determined by a modification of the method of Klaidman *et al*. (37). *E. coli* AB1157 was grown in 50 ml of K medium plus 1 μg/ml thiamine at 37 ºC to an A_{600} of ~0.5 and then H_2O_2 was added to the culture medium and incubation was continued for 15 min. Anaerobic cultures were grown with bubbling 95% N_2/5% CO_2 prior to and after H_2O_2 addition. After H_2O_2 challenge, cell pellets were collected by centrifugation and resuspended in 1M KCN, 0.3 N KOH, 5 mM EDTA and then mixed with an equal volume of 50 mM tributylammonium bicarbonate, pH 10, to give a final volume of ~2.5 ml. The lysate was cleared

by centrifugation, filtered through a 0.2 μm filter, and analyzed by HPLC. Amounts of nicotinamide nucleotides were determined by measuring areas of the HPLC peak traces at 327 nm and comparing these to standard 3 nmol samples of each of the nicotinamide nucleotides run under identical conditions. Sample traces are given in the supplementary data (Fig. S1). Cellular concentrations were calculated assuming that an OD_{600} = 1.0 corresponds to 10^9 cells/ml and that the volume of a cell is 10^{-12} ml (38).

Metal Titrations of NADH and its Analogs Monitored by NMR Spectroscopy – NMR spectra of freshly-prepared 0.5 ml solutions of NAD(P)H, NMNH, or ADP-ribose between 10 and 100 mM in D_2O, pD ~ 7.5, were acquired after incremental addition of $FeCl_3 \cdot 6\ H_2O$ or $Ga(NO_3)_3$ in D_2O as indicated. Addition of DCl at pH 2.5 to a D_2O solution of NADPH in the same amounts as those added for Fe^{3+} or Ga^{3+} resulted in no significant shifting of the NMR resonances. Spectra were acquired within 30 min of Fe^{3+} addition. Percent broadening of NMR resonances upon addition of Fe^{3+} was calculated using the formula

$$100 \times [1\text{-(peak height with } Fe^{3+})/(\text{initial peak height})].$$

A broadening of 100% indicates that no resonance was visible. K_d values and fractional occupancy of Ga^{3+} were determined as described previously (39). Percentages of NAD(P)H in linear and folded forms were calculated as described by Oppenheimer *et al.* (40).

Elemental Analyses of Ga^{3+}/NAD(P)H Precipitates – Twenty mg of NAD(P)H were dissolved in 0.4 ml H_2O and 1 equivalent of $Ga(NO_3)_3$ in 7.5 μl was added. A white precipitate formed immediately for the NADH sample, but an additional 1 equivalent of $Ga(NO_3)_3$ was added to the NADPH sample to obtain sufficient precipitate for analysis. Both samples were centrifuged at 14,000 rpm for 5 min, and the supernatant was discarded. The precipitates were washed three times by centrifugation with 1 ml water and dried under vacuum.

For the NADH sample, the best-fit formula was $Na[(NADH)Ga_2(OH)_5] \cdot 3\ H_2O$; Anal. calc. (found): C 26.1 (26.7), H 3.97 (3.87), N 10.2 (10.1), Ga 14.5 (13.7). For the NADPH sample, the best-fit formula was $Na_{0.7}[(NADH)Ga_{2.3}(OH)_{3.6}] \cdot 4\ H_2O$; Anal. calc. (found): C 24.0 (23.4), H 3.61 (3.40), N 9.33 (8.90), Ga 15.3 (15.7).

Metal Titrations of NAD(P)H Monitored by Absorbance Spectroscopy – Absorbance spectra of freshly-prepared solutions of NAD(P)H were acquired after incremental addition of $Fe(NO_3)_3$ to 50 μM or 500 μM solutions of NAD(P)H, or $Ga(NO_3)_3$ to 66 μM solutions of NADPH. All spectra were acquired within 30 min of M^{3+} addition.

Kinetic Measurements of NAD(P)H Oxidation – Freshly-prepared solutions of 16 μM NAD(P)H were brought to 100 mM ethanol, 1.25 μM H_2O_2, and/or 80 μM $FeCl_3$ as indicated. A_{340} was measured at 25°C every 0.2 s for 7 min and corrected with appropriate blanks. Best-fit lines were calculated from the initial rates. For anaerobic measurements, the water used to prepare the samples was degassed with argon for 3 h prior to use, and the samples were prepared and sealed under an argon atmosphere. The initial rates were very dependent on concentration, so care was taken to use the same solutions and order of addition of reactants for both the NADH and NADPH trials.

Molecular Modeling – Molecular models for Fe^{3+} binding to NADPH were constructed using Spartan '02 (Wavefunction, Inc., Irvine, CA). The NADPH conformation was obtained from the most probable folded conformation as predicted by NMR spectroscopy (41): 4'-5' gg and 5'-O gg rotamers for both the adenyl and reduced nicotinamide ribose units, 2'-endo conformation for the nicotinamide ribose, and 3'-endo conformation for the adenine ribose. To ensure that the molecule remained in the folded conformation, the distance between the adenine and reduced nicotinamide rings was restrained to 3.6 Å. This NADPH conformation was energy-minimized using MMFF94 force field calculations (42) before adding the Fe^{3+} ion at a restrained distance of 2.1 Å (43) to the adenine N7. Because of steric hindrance due to the close contacts between the adenine-N7-bound Fe^{3+} and the adenine amino group, a bond between the Fe^{3+} and the amino group was included and restrained to a distance of 2.3 Å.

RESULTS

Nicotinamide Nucleotide Enzyme Levels After H_2O_2 Challenge of E. coli – Because of a possible involvement of NAD(P)H in mediating H_2O_2 toxicity, the activities of several enzymes involved in nicotinamide nucleotide metabolism (Table I) were measured before and after challenge with H_2O_2 (Table II). In consideration of the existence of the "early" H_2O_2 induction of proteins, the activities of which are induced during the first 10-18 min but return to normal within 30 min following the addition of hydrogen peroxide (44), the activities were measured 15 min after challenge of catalase-deficient cells with 50 μM H_2O_2. Catalase is the major enzyme for removing hydrogen peroxide, but catalase-deficient mutants are not more sensitive to killing by H_2O_2 than are wild type cells (22). Thus, catalase mutants were used in this study to elucidate other defense systems against hydrogen peroxide. *E. coli* glucose-6-phosphate dehydrogenase (G6PD), which specifically reduces $NADP^+$, is one of the major sources of cellular NADPH. Upon H_2O_2 challenge, the activity of G6PD was induced by about 2.9-fold (Table II). Meanwhile, the activity of isocitrate dehydrogenase, which also reduces $NADP^+$, was not induced.

NADH/$NADP^+$ transhydrogenases reversibly transfer a hydrogen atom between NADH and $NADP^+$ (Table I). Upon membrane energization either by respiration or by ATP hydrolysis, the rate of reduction of $NADP^+$ by NADH is increased several-fold, and the equilibrium constant for the reaction increased from 0.79 for the non-energy-dependent reaction to 480 (45). Presumably the physiological function of these transhydrogenases is to provide NADPH for biosynthesis and detoxification (46). To investigate whether either of these energy-linked transhydrogenase activities are increased upon hydrogen peroxide exposure, they were assayed in catalase-deficient *E. coli* cells after exposure to 50 μM H_2O_2 for 15 min (Table II). The assays included an NADH-regenerating system. The respiration-driven transhydrogenase activity was increased almost three-fold, but the ATP-dependent transhydrogenase activity showed no increase. Likewise, no induction of NADH dehydrogenase activity was observed.

In addition to alkyl hydroperoxidase (19) and *o*-dianisidine peroxidase (47), *E. coli* contains a NADH-dependent peroxidase (33). Whereas the former enzymes do not utilize H_2O_2 as substrate, the latter one does. The NADH-dependent peroxidase activity was elevated by only 38% following exposure to peroxide. However, NADPH-dependent peroxidase activity increased by 248% upon H_2O_2 challenge. NADH and NADPH oxidase activities were induced to only 140% of normal activity.

The turnover of NAD^+ is very rapid in the cell, and it is four-fold faster under aerobic conditions than anaerobic conditions (48). Moreover, in mammalian cells, DNA breaks caused by oxidative stresses can deplete NAD^+ *via* the NAD^+ glycohydrolase activity of poly(ADP-ribose) polymerase, whereas in *E. coli*, DNA ligase hydrolyzes NAD^+. Thus, it was proposed that the turnover of NAD^+ might have important functions under conditions of oxidative stress (48). Three enzymatic activities initiate NAD^+ turnover in *E. coli*: NAD^+ glycohydrolase, NAD^+ pyrophosphatase, and DNA ligase. However, none of these enzymes' activities changed following hydrogen peroxide exposure (Table II). Finally, NAD^+ kinase activity was unchanged. In conclusion, the changes in the enzyme activities indicate that H_2O_2 is depleted by NADPH-dependent peroxidases in the absence of catalase and predict that cellular NADPH levels might be increased relative to those of NADH.

Measurement of Nicotinamide Nucleotide Pools in E. coli – The determination of nicotinamide nucleotide pools is complex due to the sensitivity of NAD(P)H to degradation or oxidation during isolation. Lundquist and Olivera (49) estimated the concentrations of $NAD(P)^+$ in *E. coli*, but did not include the reduced nicotinamide nucleotides. Bochner and Ames (50) used an acid extraction procedure for purification of the nicotinamide nucleotides which probably resulted in oxidation of NAD(P)H prior to quantitation. Therefore, we modified the method used for brain cells by Klaidman *et al.* (37) to measure the effect of oxidative stress upon the free pools in *E. coli* (Table III). Cells were lysed by NaOH in the presence of cyanide and EDTA. EDTA serves to chelate metal ions that could oxidize NAD(P)H, while cyanide forms

adducts with $NAD(P)^+$ to stabilize these species against degradation in basic solution, and these adducts can conveniently be quantitated by absorbance at 327 nm.

Prior to exposure to H_2O_2, NADPH accounted for 2% and 7% of the free nicotinamide nucleotides in aerobically-grown or anaerobically-grown *E. coli*, respectively. Fifteen minutes after exposure to 0.5 mM H_2O_2, however, the NADPH level increased by about half, while the NADPH:NADH ratio increased by 5.7-fold. After exposure to 5.0 mM H_2O_2, the effects were even more dramatic: although the steady-state level of NADPH dropped to half and the ratio of NADP(H) to NAD(H) remained unchanged, the ratio of NADPH to NADH increased by 92-fold. After exposure to 10mM H_2O_2, the concentration of NADH dropped below the detectable level. Clearly, the reduced pools dramatically shift to favor NADPH under oxidative stress, which correlates well with the induced activity of NADPH-generating enzymes and NADPH-dependent peroxidases after oxidative stress.

Kinetics of NAD(P)H Oxidation by Fe^{3+} – The shift in reduced nicotinamide nucleotide pools from NADH to NADPH during oxidative stress could indicate that NADH can reduce Fe^{3+} to Fe^{2+} more rapidly than NADPH, and therefore drive the Fenton reaction more efficiently than NADPH. To test this hypothesis, the initial rates of NADH and NADPH oxidation by Fe^{3+} were determined (Table IV). Because dioxygen can gain an electron to form the superoxide radical, which is itself capable of promoting oxidative damage (51), the reactions were measured under both aerobic and anaerobic conditions.

Under anaerobic conditions, the rate of NADH oxidation by Fe^{3+} was 5.5-fold faster than that of NADPH, while under aerobic conditions, the initial rates were slightly faster, and NADH remained the preferred substrate by roughly 6-fold (Table IV). When H_2O_2 was added to the reaction, the oxidation rates increased dramatically, and the initial oxidation rate of NADH was 16-fold that of NADPH. These rates decreased only slightly in the presence of 100 mM ethanol, which can quench free hydroxyl radical (10), indicating that free hydroxyl radicals were not a major reactant in the oxidation. The presence of organic material that could effectively compete for freely diffusable hydroxyl radical might resemble the cellular environment more closely.

Thus, altering the reductant pool to favor NADPH over NADH under oxidative stress would result in a major decrease in the potential to reduce Fe^{3+} and hence in levels of Fe^{2+}-generated oxidants.

Analysis of Complexes of NAD(P)H with Fe^{3+} and Ga^{3+} by NMR Spectroscopy – NADH and NADPH differ only by the presence of a 2'-phosphate group on the adenine ribose of NADPH. Their structural properties in solution are also similar, with both molecules existing in an equilibrium between an extended form, in which the reduced nicotinamide ring and the adenine ring at opposite ends of the molecule, and a folded conformation in which the two hydrophobic rings are stacked (41). At 22°C, 36% of either species is in the folded form (40). In addition, the reduction potentials of the two molecules are nearly identical (0.32 V; (52)). Thus the different rates of oxidation by Fe^{3+} must be due to different localization of Fe^{3+} on the nucleotides, to an electronic difference by which the 2'-phosphate raises the energy of an electron transfer to Fe^{3+}, and/or to a shift in equilibrium between the linear and folded conformations.

To study such differences, NMR titrations of NADH and NADPH with Fe^{3+} were carried out. Titrations were also done with Ga^{3+}, which is similar to Fe^{3+} in ionic radius (0.645 and 0.620 Å, respectively; (53)), and has a similar hydrolysis equilibrium constant for the association of aqua ligands (pK_h = 2.6 and 2.2, respectively; (54)). (The pK_h reflects the tendency of metal ions to coordinate to hard donor atoms such as oxygen *versus* softer donor atoms such as nitrogen.) In addition, both Ga^{3+} and Fe^{3+} are labile metals with ligand exchange occurring at the rate of 403 and 160 s^{-1}, respectively (55). One important difference between these metal ions, however, is that Ga^{3+} has no unpaired electrons and is therefore diamagnetic, as opposed to the paramagnetic high-spin Fe^{3+} that has five unpaired electrons. This property of Ga^{3+} makes it ideally suited to NMR studies at high metal ion concentrations (56-59), whereas Fe^{3+} can be utilized effectively only at very low concentrations due to paramagnetic broadening of the resonances. One advantage of the Fe^{3+} paramagnetic broadening of NMR resonances, however, is the ability to determine Fe^{3+} localization in the molecule, since signal broadening is proximity-

dependent. Finally, Ga^{3+} cannot be reduced to Ga^{2+}, so binding could be studied independently of metal ion reduction.

In studies of ATP, dAMP and calf thymus DNA, the adenine ring was observed to contain two favored metal-ion binding sites, the adenine N1 and N7 atoms (60-62). In the case of ATP, N1 is the predominate localization site only at pH 3-4.5, while binding of Fe^{3+} to the adenine N7 is favored at neutral pH (60). When we examined broadening of the proton resonances by Fe^{3+} of 10 mM ADP-ribose (a molecule similar to NADH but lacking a nicotinamide ring) with 0.01, 0.05 and 0.10 equivalents of Fe^{3+}, broadening was slightly greater for the adenine H8 proton than for the H2 proton. This differential broadening indicates that Fe^{3+} interaction with the adenine N7 site was slightly stronger than with N1 (Fig. 1). Analysis of additional ribose resonances was not possible due to the highly overlapping signals from the α and β anomers of this compound. Examining the proton broadening of 10 mM NMNH with 0.01 and 0.05 equivalents of Fe^{3+} or 50 mM NMNH with 0.05 equivalents of Fe^{3+}, only general proton resonance broadening was observed with little selectivity (Fig. 2A-C).

When a comparison was made for Fe^{3+}-induced proton resonance broadening for NADH and NADPH (Fig. 2) at 10 mM nucleotide and 0.01 equivalents of Fe^{3+} (Fig. 2A, Fig. 3), strongly selective broadening occurred for the adenine H8 proton of NADH, but only slight broadening was seen for the adenine H8 proton of NADPH. Meanwhile, sharpening was observed for the adenine H2 proton of NADPH, but not the adenine H2 proton of NADH. This signal sharpening is most likely a result of conformational change in the molecule upon metal ion addition. Less broadening of the reduced nicotinamide ring and nicotinamide ribose protons was also observed for NADPH than NADH. In essence, these results indicate that the adenine N7 is the major site for Fe^{3+} binding to NADH (as was the case for ATP), but for NADPH there was no binding to the adenine N1 and less general binding to the reduced nicotinamide ring and the nicotinamide ribose. The smaller broadening seen for the H8 resonance of NADPH might indicate that, at lower Fe^{3+} concentrations, Fe^{3+} is localizing at this site to a lesser extent.

These conclusions were confirmed with 10 mM nicotinamide nucleotide and 0.05 equivalents of Fe^{3+} (Fig. 2B, Fig. 3). With NADH there was general broadening, but with NADPH there was less binding of the adenine N1 (as observed by the smaller amount of broadening at the adenine H2 proton) and less broadening of the reduced nicotinamide and nicotinamide ribose protons. Finally, at 100 mM nucleotide and 0.01 equivalents of Fe^{3+} (50 mM NMNH), the most notable effect was reduced broadening of the nicotinamide protons for NADPH *versus* NADH (Fig. 2C). It should be noted that at 0.05 equivalents of Fe^{3+}, general broadening of all NMR resonances was observed, both because of the higher Fe^{3+} concentration and because of the formation of radical species as Fe^{3+} oxidized the nucleotides. Such broadening was most noticeable for NADH (Fig. 2) due to the faster rate of NADH oxidation. For ADP-ribose, which cannot be oxidized, addition of up to 0.10 equivalents of Fe^{3+} showed only selective resonance broadening (Fig. 1), as compared to the general broadening seen for NADH (Fig 2).

^{13}C NMR resonance broadening (Fig. 2D) suggests that Fe^{3+} localizes near the nicotinamide amide of NADH (as observed by broadening of the nicotinamide C7 resonance). This selectivity was somewhat less for NADPH, and absent for NMNH. It should be noted that this Fe^{3+} interaction at the nicotinamide C7 is seen primarily at the high concentrations (100 mM) necessary to obtain ^{13}C NMR spectra. Likewise, broadening of the carbon resonances on the adenine ring is stronger for NADH than NADPH (Fig. 2D), indicating greater interaction of Fe^{3+} with the adenine ring of NADH than that of NADPH. Addition of 0.01 equivalents of Fe^{3+} also resulted in extreme broadening of the phosphorus resonances (> 80%) of the pyrophosphate backbone of NADH and NADPH and the 2'-phosphate of NADPH (data not shown), indicating that Fe^{3+} also localizes at the negatively-charged phosphate groups.

Addition of Ga^{3+} to solutions of NADH resulted in the immediate formation of a white precipitate, preventing NMR studies. However, addition of Ga^{3+} to NADPH solutions resulted in precipitate formation only at high concentrations. As noted in Experimental Procedures, elemental analysis of the precipitates indicated that they contained roughly two Ga^{3+} per

NAD(P)H molecule. Evidently, Ga^{3+} coordinates to NAD(P)H, most likely at the negatively-charged pyrophosphate backbone, creating a neutral, insoluble species. Despite the difficulty with precipitation, spectra of NADPH were obtained from ^{1}H NMR titrations with up to two equivalents of Ga^{3+} (Fig. 4A). Significant shifting of the adenine H8 and H2 resonances as well as the adenine ribose H2' resonance was observed with increasing Ga^{3+} concentration, suggesting that Ga^{3+}, like Fe^{3+}, localizes around the adenine N7 and N1, though in this case with roughly equal affinity at the two sites. Above 1.5 equivalents of Ga^{3+} signal broadening occurred due to precipitation.

Interaction of Ga^{3+} with NADPH was also examined with ^{31}P NMR (Fig. 4B). Strong shifting of the 2'-phosphate resonance was observed (δ = 3.9) up to 1.0 equivalent of Ga^{3+}, whereas the pyrophosphate shifting was relatively weak (δ = 0.12). Consistent shifting of the 2'-phosphate resonance occurred with Ga^{3+} up to 0.8 equivalents, as seen also for shifting of the adenine ribose H2' resonance (Fig. 4A). Shifting of the latter resonance indicates that the Ga^{3+} has a high affinity for this site in addition to the adenine N7 and N1 sites. Also noteworthy in the pyrophosphate backbone resonance at high equivalents of Ga^{3+} is a small shift from a single resonance into two distinguishable peaks, indicating that the two phosphorous atoms become chemically inequivalent. Such splitting could indicate that one oxygen atom of only one of the backbone phosphates was coordinating a Ga^{3+} ion. In contrast, similar experiments with NMNH indicated that Ga^{3+} did not localize on the reduced nicotinamide ring, but only at the terminal phosphate group. A complete table of the ^{1}H, ^{13}C, and ^{31}P NMR resonance broadening for Ga^{3+} titrations with NADPH and NMNH is given in the supporting information (Table S1).

Our interpretation of the NMR results are summarized schematically in Fig. 5. Both NADH and NADPH have major Fe^{3+} binding sites at the adenine N7. NADH also has weaker interactions with adenine N1 and the reduced nicotinamide ring. In contrast, NADPH shows strong binding at the 2'-phosphate group, presumably at the expense of binding to the adenine N1 and reduced nicotinamide ring, and to a lesser extent, the adenine N7. In essence, the 2'-

phosphate group of NADPH diminishes interactions with the less-specific sites seen for NADH, as expected for the addition of a strong site for Fe^{3+} localization.

Estimation of K_d for NADPH and Ga^{3+} – Due to the broadening of NAD(P)H NMR resonances by Fe^{3+} at sub-stoichiometric amounts, K_d values could not be calculated for this interaction. However, a K_d for Ga^{3+} interactions with NADPH could be estimated from ^1H NMR Ga^{3+} titration data of 1 mM NADPH (Fig. 6A). Fitting the shifts in the adenine ribose 2'-phosphate resonance for a one-site binding model, the K_d was calculated to be approximately 550 μM (Fig. 6B). Given this K_d, the percentage of 1 mM Ga^{3+} bound to 1 mM NADPH at the 2'-phosphate was calculated to be 48%. Because the 2'-phosphate is a relatively strong site of metal ion localization, this could be close to the total amount of NADPH-bound Ga^{3+}.

Analysis of Complexes of NAD(P)H with Fe^{3+} and Ga^{3+} by Absorption Spectroscopy – The absorption spectra during a titration of 50 μM NADH or NADPH with Fe^{3+} are shown in Figure 7. The absorption band at 260 nm is primarily due the adenine ring with a small contribution from nicotinamide ring, whereas the less intense band near 340 nm is solely due to the nicotinamide ring (63). Addition of Fe^{3+} to either NADH (Fig. 7A) or NADPH (Fig. 7B) resulted in a decrease in the absorption at 340 nm and a shift of the maximum to higher wavelengths (lower energy). The hypochromism and bathochromic shift are likely due to the formation of a charge-transfer species with Fe^{3+} that perturbs the energies of the reduced nicotinamide molecular orbitals. Similar hypochromic effects have been observed for the binding of metal complexes to DNA (64,65). Titration of NADPH with Ga^{3+} under the same conditions (supporting information, Fig. S2) caused no shift in the 340 nm band and Ga^{3+} cannot form charge-transfer complexes. Only very slight hypochromicity (6%) was observed during the Ga^{3+} titration, suggesting that most of the change in the NAD(P)H absorption spectra was brought about by Fe^{3+} results from the charge transfer complex formation.

The changes in A_{340} of NADH and NADPH as a function of Fe^{3+} concentration (Fig. 7B, inset), indicates that the interactions of Fe^{3+} with the two nucleotides differ considerably. While the A_{340} of NADH decreased steadily with increased Fe^{3+}, the A_{340} for NADPH reproducibly

showed a rapid decrease then became constant. These differences suggest the presence of a second Fe^{3+} binding site peculiar to NADPH, presumably the 2'-phosphate group, or alternatively, that the charge-transfer complexes might differ for the two nucleotides. Indeed, absorption spectra at higher (500 μM) concentrations of nucleotides in the presence of Fe^{3+} exhibited absorbance maxima at 520 nm for NADPH and at 544 nm for NADH (supporting information, Fig. S3), indicating a difference between the two charge transfer complexes. These absorbances were maximal at 0.5 equivalents of Fe^{3+} and decreased over time.

Gutman *et al*. reported a charge-transfer band at 540 nm for both the $(NADH)_2Fe^{3+}$ and $(NADPH)_2Fe^{3+}$ complexes (66,67). Those experiments, however, were performed at pH 3.5 at which the pyrophosphate backbone oxygen atoms and two of the 2'-phosphate oxygen atoms of NADPH would have been protonated. Differential protonation of NAD(P)H in the respective experiments is the likely explanation for the changes in wavelength of the charge transfer bands seen in our studies. In addition, while the charge-transfer absorbances observed here at pH 7.5 for NADPH (66) are approximately the same as reported by Gutman *et al.* (ε = 800 *versus* 900 $cm^{-1}M^{-1}$, respectively), the absorbances observed for NADH (67) are half as intense (ε = 400 *versus* 875 $cm^{-1}M^{-1}$, respectively). With the differences in pH and a partial occupancy of 20% for the Fe^{3+} binding to NAD(P)H, assuming that the K_d of the Ga^{3+} and Fe^{3+} interactions are similar, the different intensity of these charge transfer bands is not surprising.

The energy difference between the NADPH/Fe^{3+} and NADH/Fe^{3+} charge transfer bands was calculated to be 2.4 kcal/mol, indicating that the charge transfer species is lower in energy for NADH than for NADPH. Therefore, the rate for the reduction of Fe^{3+} to Fe^{2+} could be as much as 60-fold greater for NADH than for NADPH. This is consistent with the fact that oxidation rates of NADPH are up to 16-fold slower than those of NADH in the presence of Fe^{3+}.

An Energy-Minimized Structural Model for the Complex of Fe^{3+} with the Adenine Ring of NADH and NADPH – Based on the NMR and absorbance studies, a model for the interaction of Fe^{3+} with the adenine ring of NAD(P)H was constructed (Fig. 8). The most probable configuration of NAD(P)H as reported by Oppenheimer (40) was used as the starting structure

for the folded conformation of the molecule, and then Fe^{3+} was placed at a distance of 2.1 Å from the adenine N7 (43). Because of steric hindrance between the bound Fe^{3+} and the adenine amino group which was encountered in the refinement of the model, a second bond between the Fe^{3+} and the amino group (2.3 Å) was added. The adenine amino protons are not observable by NMR spectroscopy, so direct M^{3+} interactions at this site cannot be observed. However, studies of M^{2+} interactions with adenine analogs showed significant interactions between the metal ion and the neighboring amino group (68). Attempts to add a Fe^{3+} ion bound to the adenine N1 resulted in severe steric hindrance with the adenine amino group, so it is not surprising that Fe^{3+} localization at this site was weaker than for adenine N7.

To keep the model in a stacked conformation, the distance between the reduced nicotinamide ring and the adenine ring was restrained to 3.6 Å. Although the Fe^{3+} is bound to the adenine ring and not to the redox-active nicotinamide ring, the folded form of the molecule presumably brings the reduced nicotinamide ring close enough to the Fe^{3+} to promote electron transfer. From analysis of the NMR spectra of NADPH/Ga^{3+}, the percentage of NADPH in the folded conformation does not change upon metal ion addition (as determined using the method described in Experimental Procedures), so the metal ion apparently does not hold the adenine and reduced nicotinamide rings in close proximity. The effect of Fe^{3+} on the folded/linear equilibrium of NAD(P)H could not be measured due to the relatively low equivalents of Fe^{3+} used in these titrations.

In solution at pH 7.5, the Fe^{3+} ion would have octahedral geometry, most likely binding a combination of water molecules and/or hydroxyl ions to complete the coordination sphere. In addition to interactions at the adenine N7 and the amine, it is also possible that one of the oxygen atoms from the pyrophosphate backbone could coordinate the Fe^{3+}, which would explain the inequivalency seen for the backbone phosphorus atoms at high Ga^{3+} concentration in the NADPH ^{31}P NMR titration (Fig. 3B).

As can be seen from Fig. 8, Fe^{3+} bound to the 2'-phosphate group of the NADPH would be directed away from the adenine N7 binding site and hinder charge transfer from the reduced

nicotinamide ring even in the stacked conformation. Of course, this model applies to the strong binding site of Fe^{3+} at the adenine N7, not to the other, weaker binding sites whose interactions are significantly diminished by the presence of the 2'-phosphate of NADPH.

DISCUSSION

Exposure of *E. coli* to H_2O_2 induced the activity of G6PD and the respiration-dependent NADH/$NADP^+$ transhydrogenase, enzymes which synthesize NADPH. Additionally, activities of NADH-dependent oxidase and peroxidase as well as NADPH-dependent oxidase increased by about half, but NADPH-dependent peroxidase activity increased by 2.5-fold. These changes are consistent with the large measured increase in the ratio of the NADPH/NADH pools and with NADPH being a much slower reductant of Fe^{3+} than is NADH. This satisfying correlation between the induction of enzymes to produce NADPH, the increase in NADPH relative to NADH, and the much lower reactivity of NADPH with Fe^{3+} suggests that these changes are a cellular strategy to protect against oxidative damage, and indirectly suggests that NADH is a primary cellular reductant responsible for reduction of Fe^{3+} to drive the Fenton cycle *in vivo*. NAD(P)H may not be solely responsible for the reduction of Fe^{3+} to Fe^{2+} and driving the production of reactive oxygen species, however, as reduced flavins have been implicated as reductants that drive the Fenton cycle, at least in non-respiring *E. coli* cells (69). Nonetheless, we propose that in respiring cells the regulation of NADH and NADPH levels under oxidative stress conditions may enhance survival by storing reducing potential in the form of NADPH.

Consistent with our proposal, the induction of G6PD by H_2O_2 supports a growing understanding of the major role for this enzyme in defense against oxidative stress. G6PD deficiency in humans due to point mutations in the G6PD gene results in the loss of intracellular NADPH and an enhanced sensitivity to oxidants (25). Persons carrying the mutations exhibit hemolytic anemia under conditions of oxidative stress by exogenous agents or infection (70). Severely impaired catalase activity resulting from the decrease in NADPH was proposed to be an underlying mechanism of oxidant susceptibility in these individuals (71). However, catalase-

deficient humans show only minor adverse physiological effects such as an increased risk of diabetes (72).

In *G6PD* null strains of mice or yeast, other NADPH-generating enzymes such as isocitrate dehydrogenase do not seem to compensate for the loss of G6PD in defenses against oxidative damage. Consistent with this observation, the activity of isocitrate dehydrogenase was not induced when *E. coli* was challenged with H_2O_2. Despite this lack of induction in *E. coli*, increasing the level of $NADP^+$-dependent isocitrate dehydrogenase was found to increase resistance to oxidative damage of transformed mouse fibroblasts (73).

Zheng *et al.* (74) used DNA microarray analysis to profile transcriptional responses to hydrogen peroxide in *E. coli.* They listed the thirty most highly-induced genes which showed levels of induction of more than ten-fold. Eleven of these genes had unknown function, while none of the remaining nineteen overlapped those whose protein activities were measured here. Of course, changes in transcript levels do not translate directly to changes in enzyme activity for a number of reasons, so that both approaches are necessary in order to obtain a comprehensive understanding of the responses to oxidative stress.

Because of the structural similarity of NADH and NADPH, the cause of the large difference in the rate of Fe^{3+} reduction between them must be the 2'-phosphate group on NADPH. The NMR data for both showed that M^{3+} ions localized primarily on the adenine N7 (and the nitrogen of the adenine amino group), with secondary interactions at the amide group of the reduced nicotinamide ring, the adenine N1, and the oxygen atoms in the pyrophosphate backbone. For NADPH, M^{3+} ions also localized on the 2'-phosphate group, as would be expected from the negative charge of this group. The presence of this 2'-phosphate on NADPH decreased metal binding at the adenine N7, N1 and the reduced nicotinamide ring as compared to

NADH. Since separate K_d measurements for M^{3+} association with the adenine N7 and the 2'-phosphate of NADPH could not be obtained, a direct comparison of strength of M^{3+} binding to these sites cannot be made. It is reasonable to assume, however, that metal ion binding at these two sites is competitive. The Fe^{3+} ion, when bound to the adenine N7 and the amino group, does not simultaneously bind the reduced nicotinamide ring, as evidenced by the NMR data. However, the equilibrium between the linear and folded forms of NAD(P)H would bring the reduced nicotinamide ring into close proximity of the adenine ring, enabling Fe^{3+} reduction.

It is also conceivable that the 2'-phosphate could change the electronic configuration of the nicotinamide nucleotide and increase the energy required to transfer an electron from NADPH to Fe^{3+} as compared to NADH. Evidence for the higher energy of charge transfer from NADPH to Fe^{3+} as compared to NADH was deduced from differences in the absorption spectra during titrations of NADH *versus* NADPH with Fe^{3+}. The presence of the charge-transfer band at a lower wavelength (higher energy) for NADPH indicates that the charge transfer process is energetically less favorable for NADPH than for NADH. Presently, our results indicate that both structural and electronic differences between NADPH and NADH are responsible for the lower rate of Fe^{3+} reduction, and further studies are required to determine the individual contributions of these factors.

It is generally accepted that NAD^+ serves primarily for the generation of ATP, whereas NADPH serves primarily as an electron or hydride donor in reductive biosynthetic reactions. We propose an additional purpose for the ubiquitous existence of the two similar nicotinamide nucleotides: by increasing the NADPH:NADH ratio under oxidative stress, an order of magnitude decrease in oxidative damage to cellular components *via* iron-mediated Fenton oxidants would result due to the slower reduction of Fe^{3+} by NADPH.

Acknowledgements – This work was supported by NIH grants RO1GM19020 and P30ES01986. J. L. B. was supported by training grant T32ES07075. We are indebted to James A. Imlay, S. Michael Chin, Yong Zhang Luo, and Leighanne Olson for providing the foundation experiments for this work. We thank Dr. Kenneth Raymond for the use of his UV-vis spectrometers.

REFERENCES

1. Chance, B., Sies, H., and Boveris, A. (1979) *Physiol. Rev.* **59,** 527-605
2. Fridovich, I. (1978) *Science* **201,** 875-880
3. Cerutti, P. A. (1985) *Science* **227,** 375-381
4. Tyrrell, R. M., and Pidoux, M. (1989) *Photochem. Photobiol.* **49,** 407-412
5. Prieto-Alamo, M. J., Abril, N., and Puyeo, C. (1993) *Carcinogenesis* **14,** 237-244
6. Barja, G. (2002) *Ageing Res. Rev.* **1,** 397-411
7. Halliwell, B. (2001) *Drugs & Aging* **18,** 635-716
8. Markesbery, W. R., and Carney, J. M. (1999) *Brain Pathol.* **9,** 133-146
9. Olsinki, R., Gackowski, D., Foksinski, M., Rozalski, R., Rozalski, K., and Jaruga, P. (2002) *Free Rad. Biol. Med.* **33,** 192-200
10. Imlay, J. A., Chin, S. M., and Linn, S. (1988) *Science* **240,** 640-642
11. Halliwell, B., and Gutteridge, J. M. C. (1990) *Methods in Enzymol.* **186,** 1-85
12. Qian, S. Y., and Buettner, G. R. (1999) *Free Rad. Biol. Med.* **26,** 1447-1456
13. Lloyd, R., Hanna, P. M., and Mason, R. P. (1997) *Free Rad. Biol. Med.* **22,** 885-888
14. Imlay, J. A., and Linn, S. (1988) *Science* **240,** 1302-1309
15. Peskin, A. V. (1996) *Free Rad. Biol. Med.* **20,** 313-318
16. Sinha, B. K., Mimnaugh, E. G., Rajagopalan, S., and Meyers, C. E. (1989) *Cancer Res.* **49,** 3844-3848
17. Mezzetti, A., Di Ilio, C., Calafione, A. M., Aceto, A., Marzio, L., Frederici, G., and Cuccurello, F. (1990) *J. Molec. Cell. Cardiol.* **22,** 935-938
18. Kirkman, H. N., and Gaetani, G. F. (1984) *Proc. Natl. Acad. Sci. USA* **81,** 4343-4347
19. McKie, J. H., and Douglas, K. T. (1991) *FEBS Lett.* **279,** 5-8

20. Hillar, A., Nicholls, P., Switala, J., and Loewen, P. C. (1994) *Biochem. J.* **300,** 531-539

21. Greenberg, J. T., and Demple, B. (1986) *J. Bacteriol.* **168,** 1026-1029

22. Imlay, J. A., and Linn, S. (1987) *J. Bacteriol.* **169,** 2967-2976

23. Demple, B., and Amabile-Cuevas, C. F. (1991) *Cell* **67,** 837-839

24. Nunoshiba, T., Hidalgo, E., Amabile-Cuevas, C. F., and Demple, B. (1992) *J. Bacteriol.* **174,** 6054-6060

25. Scott, M. D., Zuo, L., Lubin, B. H., and Chiu, D. T.-Y. (1991) *Blood* **77,** 2059-2064

26. Pandolfi, P. P., Sonati, F., Rivi, R., Mason, P., Grosveld, F., and Luzzatto, L. (1995) *Embo J.* **14,** 5209-5215

27. Nogae, I., and Johnston, M. (1990) *Gene* **96,** 161-169

28. Slekar, K. H., Kosman, D. J., and Culotta, V. C. (1996) *J. Biol. Chem.* **271,** 28831-28836

29. Bradford, M. M. (1976) *Anal. Biochem.* **72,** 248-254

30. Zercz, C. R., Moul, D. E., Gomez, E. G., Lopez, V. M., and Andreoli, A. J. (1987) *J. Bacteriol.* **169,** 184-188

31. Worthington, C. C. (1988) *Worthington manual: enzymes and related biochemicals*, Worthington Biochemical Company

32. Cavari, B. Z., Avi-Dor, Y., and Grossowicz, N. (1968) *J. Bacteriol.* **96,** 751-759

33. Coves, J., Eschenbrenner, M., and Fontecave, M. (1991) *Biochem. Biophys. Commun.* **178,** 54-59

34. Kornberg, A., and Pricer, W. E. (1950) *J. Biol. Chem.* **182,** 763-778

35. Olivera, B. M., and Lehman, I. R. (1967) *Proc. Natl. Acad. Sci. USA* **57,** 1700-1704

36. Barbieri, J. T., Moloney, B. K., and Mendo-Mueller, L. M. (1989) *J. Bacteriol.* **171,** 4362-4369

37. Klaidman, L. K., Leung, A. C., and Adams, J. D., Jr. (1995) *Anal. Biochem.* **228,** 312-317

38. Norland, S., Hedal, M., and Tumyr, O. (1987) *Microb. Ecol.* **13,** 95-101

39. Rai, P., Cole, T. D., Wemmer, D. E., and Linn, S. (2001) *J. Molec. Biol.* **312,** 1089-1101

40. Oppenheimer, N. J., Arnold, L. J., Jr., and Kaplan, N. O. (1978) *Biochemistry* **17,** 2613-2619

41. Oppenheimer, N. J. (1987) in *Pyridine Nucleotide Coenzymes* (Dolphin, D., Poulson, R., and Avramovic, O., eds) Vol. A, pp. 185-230, Wiley, New York

42. Kong, J., White, C. A., Krylov, A. I., Sherrill, D., Adamson, R. D., Furlani, T. R., Lee, M. S., Lee, A. M., Gwaltney, S. R., Adams, T. R., Ochsenfeld, C., Gilbert, A. T. B., Kedziora, G. S., Rassolov, V. A., Maurice, D. R., Nair, N., Shao, Y., Besley, N. A., Maslen, P. E., Dombroski, J. P., Daschel, H., Zhang, W., Korambath, P. P., Baker, J., Byrd, E. F. C., Van Voorhis, T., Oumi, M., Hirata, S., Hsu, C.-P., Ishikawa, N., Florian, J., Warshel, A., Johnson, B. G., Gill, P. M. W., Head-Gordon, M., and Pope, J. A. (2000) *J. Computational Chem.* **21,** 1532-1548

43. Obrey, S. J., Bott, S. G., and Barron, A. R. (2000) *J. Chem. Cryst.* **30,** 61-63

44. Storz, G., Tartaglia, L. A., Farr, S. B., and Ames, B. N. (1990) *Trends Genet.* **6,** 363-368

45. Lee, C.-P., and Ernster, L. (1964) *Biochim. Biophys. Acta* **81,** 187-190

46. Bragg, P. D., Davies, P. L., and Hou, C. (1972) *Biochem. Biophys. Res. Commun.* **47,** 1248-1255

47. Claiborne, A., and Fridovich, I. (1979) *J. Biol. Chem.* **254,** 4245-4254

48. Park, U. E., Olivera, B. M., Hughes, K. T., Roth, J. R., and Hillyard, D. R. (1989) *J. Bacteriol.* **171,** 2173-2180

49. Lundquist, R., and Olivera, B. M. (1971) *J. Biol. Chem.* **246,** 1107-1116

50. Bochner, B. R., and Ames, B. N. (1982) *J. Biol. Chem.* **257,** 9759-9769

51. Gutteridge, J. M. C., and Halliwell, B. (2000) *Ann. N. Y. Acad. Sci.* **899,** 136-147

52. Stryer, L. (1988) *Biochemistry*, 3rd Ed., W. H. Freeman & Co., New York, pp. 400

53. Shannon, R. D. (1976) *Acta Cryst.* **A32,** 751-767

54. Baes, C. F., Jr. (1976) *The Hydrolysis of Cations*, Wiley, New York

55. Hugi-Cleary, D., Helm, L., and Merbach, A. E. (1987) *J. Am. Chem. Soc.* **109,** 4444-4450

56. Kersting, B., Telford, J. R., Meyer, M., and Raymond, K. N. (1996) *J. Am. Chem. Soc.* **118,** 5712-5721

57. Stephan, H., Freund, S., Meyer, J. M., Winkelmann, G., and Jung, G. (1993) *Liebigs Ann. Chem.* 43-48

58. Wasielewski, E., Atkinson, R. A., Abdallah, M. A., and Kieffer, B. (2002) *Biochemistry* **41,** 12488-12497

59. Atkinson, R. A., Salah El Din, A. L. M., Kieffer, B., Lefevre, J.-F., and Abdallah, M. A. (1988) *Biochemistry* **37,** 15965-15973

60. Du, F., Mao, X.-A., Li, D.-F., and Liao, Z.-R. (2001) *J. Inorg. Biochem.* **83,** 101-105

61. El-Mahdaoui, L., and Tajmir-Riahi, H. A. (1995) *J. Biomolec. Struct. Dynam.* **13,** 69-86

62. Sorokin, V. A., Sysa, I. V., Valeev, V. A., Gladchenko, G. O., Degtyar, M. V., and Blagoi, Y. P. (1997) *J. Molec. Struct*. **408/409,** 233-236

63. Rizzo, V., Pande, A., and Luisi, P. L. (1987) in *Pyridine Nucleotide Coenzymes* (Dolphin, D., Poulson, R., and Avramovi, O., eds) Vol. A, pp. 99-161, Wiley, New York

64. Liu, G. D., Liao, J. P., Huang, S. S., Shen, G. L., and Yu, R. Q. (2001) *Anal. Sci.* **17,** 1031-1036

65. Cusumano, M., and Giannetto, A. (1997) *J. Inorg. Biochem.* **65,** 137-144

66. Gutman, M., Margalit, R., and Schejter, A. (1968) *Biochemistry* **7,** 2778-2785

67. Gutman, M., and Eisenbach, M. (1973) *Biochemistry* **12,** 2314-2317

68. Kapinos, L. E., Holy, A., Guenter, J., and Siegel, H. (2001) *Inorg. Chem.* **40,** 2500-2508

69. Woodmansee, A. N., and Imlay, J. A. (2002) *J. Biol. Chem.* **277,** 34055-34066

70. Gerli, G. C., Beretta, L., Bianchi, M., Agostoni, A., Gualandri, V., and Orsini, G. B. (1982) *Scand. J. Haematol.* **29,** 141-146

71. Scott, M. D., Wagner, T. C., and Chiu, D. T.-Y. (1993) *Biochim. Biophys. Acta* **1181,** 163-168

72. Goth, L., and Eaton, J. W. (2000) *Lancet* **356,** 1820-1821

73. Lee, S. M., Koh, H.-J., Park, D.-C., Song, B. J., Huh, T.-L., and Park, J.-W. (2002) *Free Rad. Biol. Med.* **32,** 1185-1196.

74. Zheng, M., Wang, X., Templeton, L. J., Smulski, D. R., LaRossa, R. A., and Starz, G. (2001) *J. Bact.* **183,** 4562-4570.

FIGURE LEGENDS

FIG. 1. **Broadening of ADP-ribose adenosine proton resonances by Fe^{3+}.** $FeCl_3 \cdot 6 H_2O$ in the equivalents shown was added to a 10 mM ADP-ribose solution and spectra were acquired as described in Experimental Procedures. The numbering scheme is given in Fig. 5.

FIG. 2. **Broadening of NAD(P)H and NMNH proton and carbon resonances by Fe^{3+}.** $FeCl_3 \cdot 6 H_2O$ was added to the nucleotide solutions and spectra were acquired as described in the Experimental Procedures. (A) ^1H NMR resonances observed with 10 mM nucleotide, 0.1 mM Fe^{3+}. (B) ^1H NMR resonances observed with 10 mM nucleotide, 0.5 mM Fe^{3+}. (C) ^1H NMR resonances observed with 100 mM NADH or NADPH and 5 mM Fe^{3+}, or with 50 mM NMNH and 2.5 mM Fe^{3+}. (D) ^{13}C NMR resonances observed with 100 mM NADH or NADPH and 1 mM Fe^{3+}, or with 50 mM NMNH and 0.5 mM Fe^{3+}. The numbering scheme for NAD(P)H is given in Fig. 5.

FIG. 3. **Broadening of the adenine ^1H NMR H8 and H2 resonances for NADH and NADPH by Fe^{3+}.** $FeCl_3 \cdot 6 H_2O$ was added to 10 mM NAD(P)H in $_{D2O}$ as indicated, and spectra were acquired as described in Experimental Procedures. With 0.01 equivalents of Fe^{3+}, broadening of the adenine H8 resonances were 54% for NADH and 11% for NADPH.

FIG. 4. **NMR titrations of NADPH with Ga^{3+}.** (A) Shifting of the adenine H8 and H2 (left) and the adenine ribose H2' (right) resonances in a ^1H NMR titration of 1 mM NADPH

with Ga^{3+} in D_2O. (B) Shifting of the 2'-phosphate (left) and pyrophosphate backbone (right) resonances in a ^{31}P NMR titration of 10 mM NADPH with Ga^{3+} in D_2O.

FIG. 5. **Conclusions for localization of Fe^{3+} upon NAD(P)H.** Sites of major broadening of ^{1}H , ^{31}P, and ^{13}C NMR resonances by Fe^{3+} are indicated in purple for (A) NADH and (B) NADPH. (C) Differences in Fe^{3+} localization upon NADPH as compared to NADH: red indicates the sites of greater Fe^{3+} localization, orange indicates sites of slightly less localization, and green indicates sites of much less localization (weak sites of interaction).

FIG. 6. **Estimation of K_d for Ga^{3+} binding to NADPH.** (A) Spectra of the adenine H8, H2 and the adenine ribose H2' resonances of NADPH (1 mM) in D_2O with Ga^{3+} added as $Ga(NO_3)_3$. (B) The K_d was determined from the shifting of the H2' resonance in the ^{1}H NMR titration of NADPH with Ga^{3+}.

FIG. 7. **Absorbance spectra of NADH and NADPH during titration with Fe^{3+}.** Nucleotide concentrations were 50 μM and Fe^{3+} was added as $Fe(NO_3)_3$ to (A) NADH or (B) NADPH. The inset shows the A_{340} values normalized to those before Fe^{3+} addition.

FIG. 8. **Energy-minimized model of Fe^{3+} bound to the adenine ring of NADPH in the folded conformation.** Fe^{3+} (yellow) is shown bound to the N7 and amine of the adenine ring. Note that the 2'-phosphate is directed away from the adenine binding site and the reduced nicotinamide ring.

TABLE I.

Enzymatic activities assayed.

Enzymes that synthesize NADPH:	
Glucose-6-phosphate dehydrogenase	D-glucose-6-phosphate + $NADP^+$ ⟶ NADPH + D-glucono-δ-lactone-6-phosphate
Isocitrate dehydrogenase	Isocitrate + $NADP^+$ ⟶ α-ketoglutarate + NADPH
$NADH/NADP^+$ transhydrogenase	
respiration-dependent	NADH + $NADP^+$ + energy produced by respiration ⟶ NAD^+ + NADPH
ATP-dependent	NADH + $NADP^+$ + ATP ⟶ NAD^+ + NADPH + ADP + P_i
Enzymes that oxidize NAD(P)H:	
In the respiratory chain:	
NADH dehydrogenase	NADH + ubiquinone ⟶ NAD^+ + ubiquinol
In the peroxidase reaction:	
NAD(P)H-dependent peroxidases	NAD(P)H + 2 H_2O_2 ⟶ $NAD(P)^+$ + 2 H_2O + O_2
NAD(P)H oxidase	NAD(P)H + O_2 + H^+ ⟶ $NAD(P)^+$ + H_2O_2
Enzymes that deplete NAD^+:	
NAD^+ glycohydrolase	NAD^+ ⟶ nicotinamide + ADP-ribose
NAD^+ pyrophosphatase	NAD^+ ⟶ NMN + AMP
DNA ligase	NAD^+ ⟶ NMN + AMP
NAD^+ kinase	NAD^+ + ATP ⟶ $NADP^+$ + ADP

TABLE II.

Changes in enzymatic activities after H_2O_2 challenge.

Cell cultures were treated with 50 μM H_2O_2 and then harvested after 15 min for assay. All measured values are the average of at least three trials. An enzymatic activity of 100% indicates no change from unchallenged cells. Numbers in parentheses are the activities before challenge.

Enzyme	Percentage Activity 15 min After Challenge
Glucose-6-phosphate dehydrogenase[a]	286 ± 28%
Isocitrate dehydrogenase	100 ± 4%
NADH/$NADP^+$ transhydrogenase[a]	
respiration-dependent	280 ± 16%
ATP-dependent	99 ± 7%
NADH dehydrogenase (ubiquitin-dependent)[a]	94 ± 8%
Peroxidase[a]	
NADH-dependent (195 U/mg)	138 ± 10%
NADPH-dependent (46 U/mg)	248 ± 29%
NAD(P)H oxidase[a]	
NADH (240 U/mg)	140 ± 13%
NADPH (39 U/mg)	145 ± 7%
NAD^+ glycohydrolase[a]	93 ± 3%
NAD^+ pyrophophatase	98 ± 7%
DNA ligase[a]	102 ± 18%
NAD^+ kinase[a]	99 ± 8%

[a]Assays were performed using catalase-deficient cells.

TABLE III.

Nicotinamide nucleotide pools 15 min after H_2O_2 challenge.

All measurements are the average of three independent experiments. In all cases, the standard deviations were less than 10 % of the mean values shown.

H_2O_2 Challenge	Nucleotide Concentrations (μM)				
(mM)	NADH	NAD^+	NADPH	$NADP^+$	NADPH/NADH Ratio
0.0 (anaerobic)	350	400	60	23	0.17
0.0	700	230	24	210	0.03
0.5	200	630	33	270	0.17
5.0	4	770	11	240	2.75
10.0	<0.1	850	8	200	>80

TABLE IV.

Rates of NAD(P)H oxidation by Fe^{3+}.

Measurements were performed at 25 °C with 160 μM NAD(P)H, as described in Experimental Procedures.

	H_2O_2 1.25 mM	$FeCl_3$ 80 μM	EtOH 100 mM	Initial rate constant (s^{-1})	Relative rate
NADH (anaerobic)	-	+	-	2.3×10^{-4}	5.5
NADH	-	+	-	2.6×10^{-4}	6.4
NADH	+	+	-	5.0×10^{-3}	120
NADH	-	+	+	2.4×10^{-4}	5.8
NADH	+	+	+	3.0×10^{-3}	72
NADPH (anaerobic)	-	+	-	4.1×10^{-5}	≡ 1.0
NADPH	-	+	-	4.2×10^{-5}	1.0
NADPH	+	+	-	3.0×10^{-4}	7.3
NADPH	-	+	+	3.2×10^{-5}	0.8
NADPH	+	+	+	2.2×10^{-4}	5.3

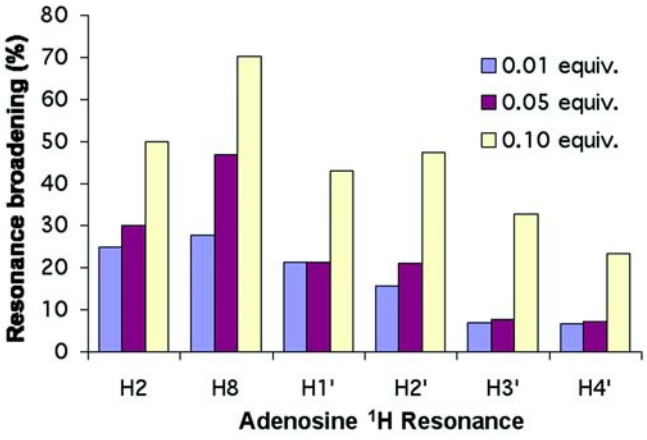

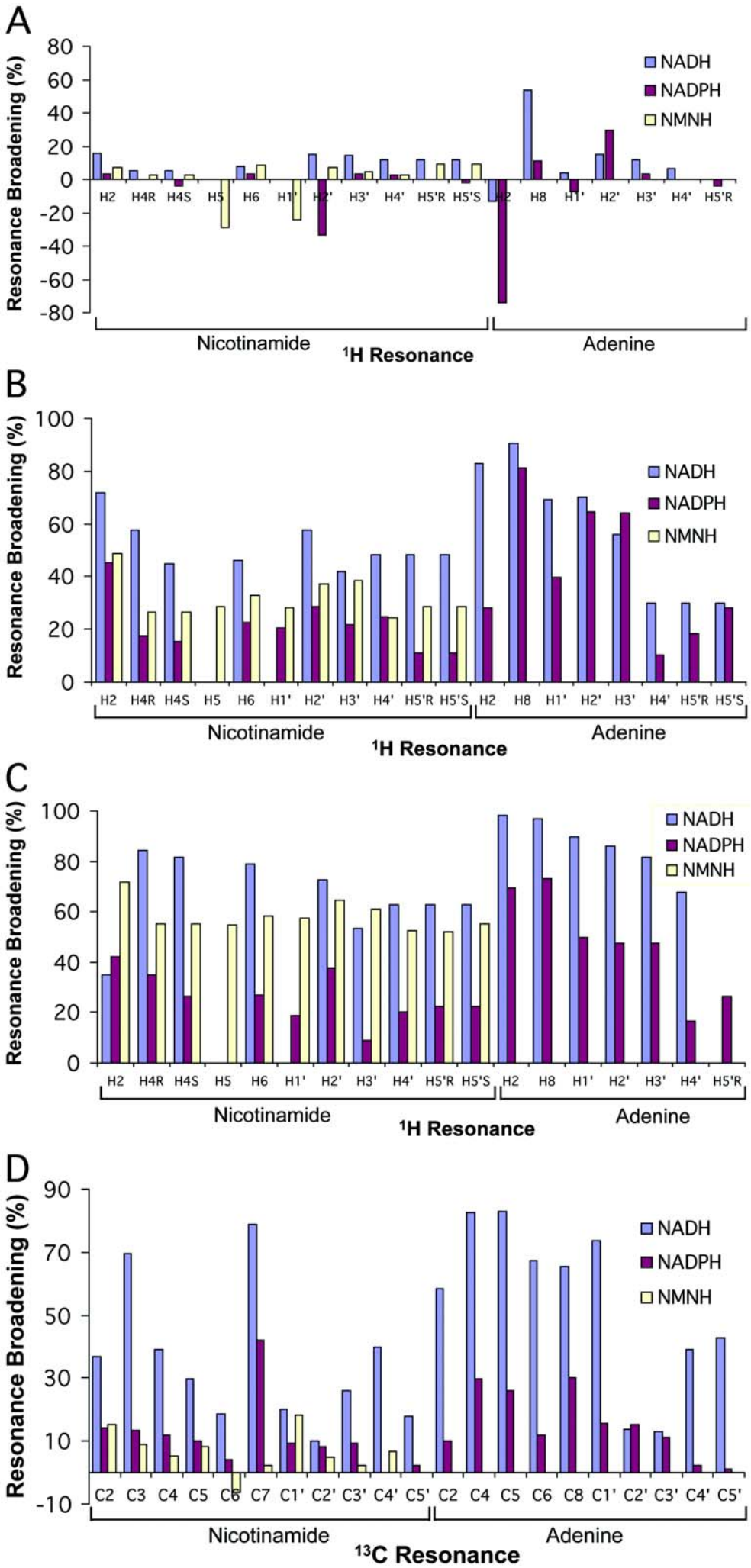

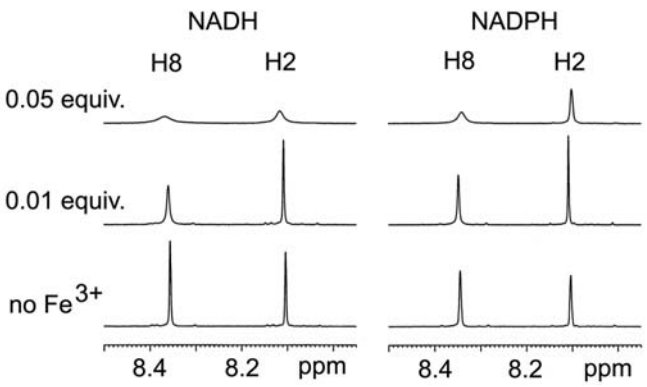

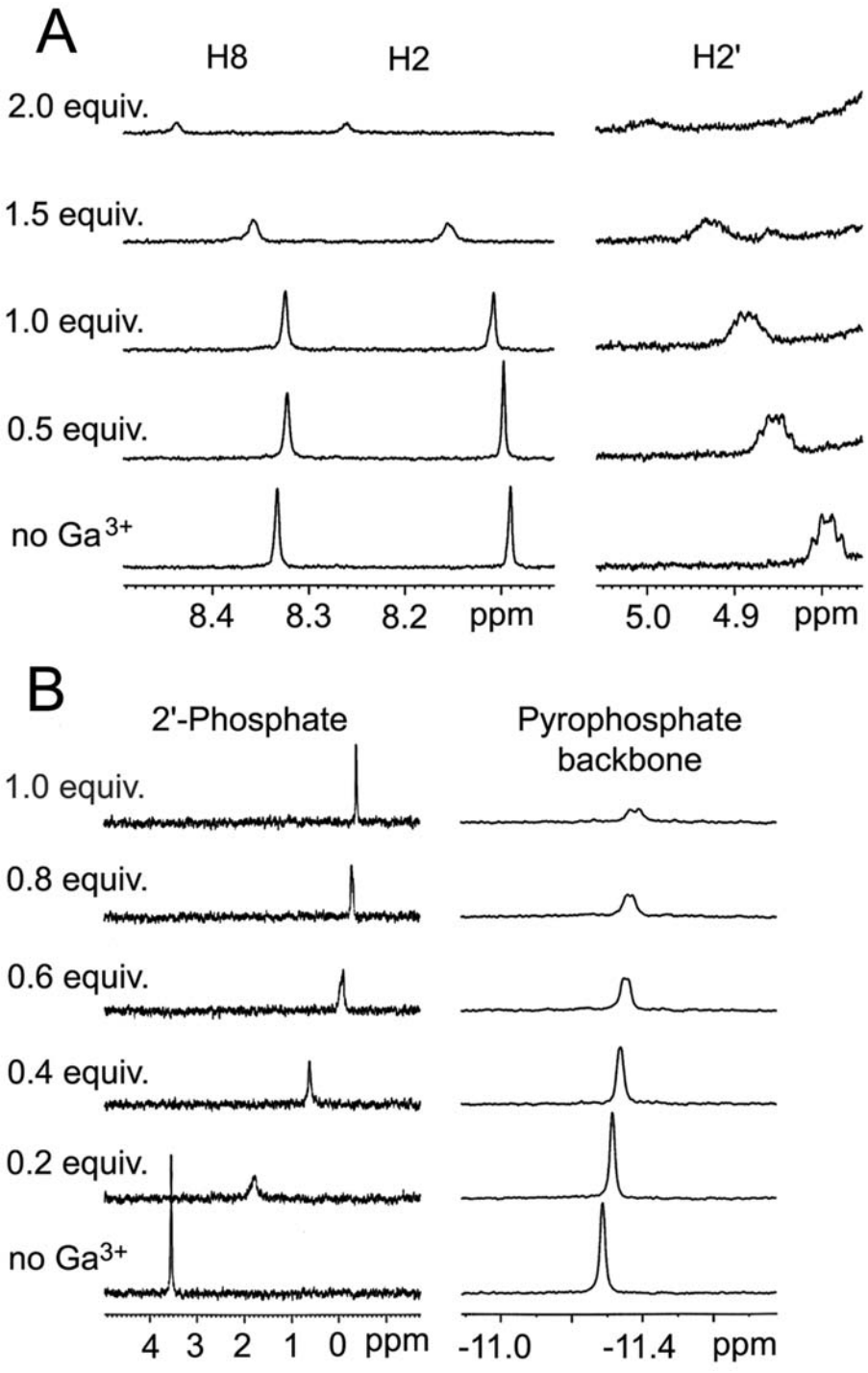

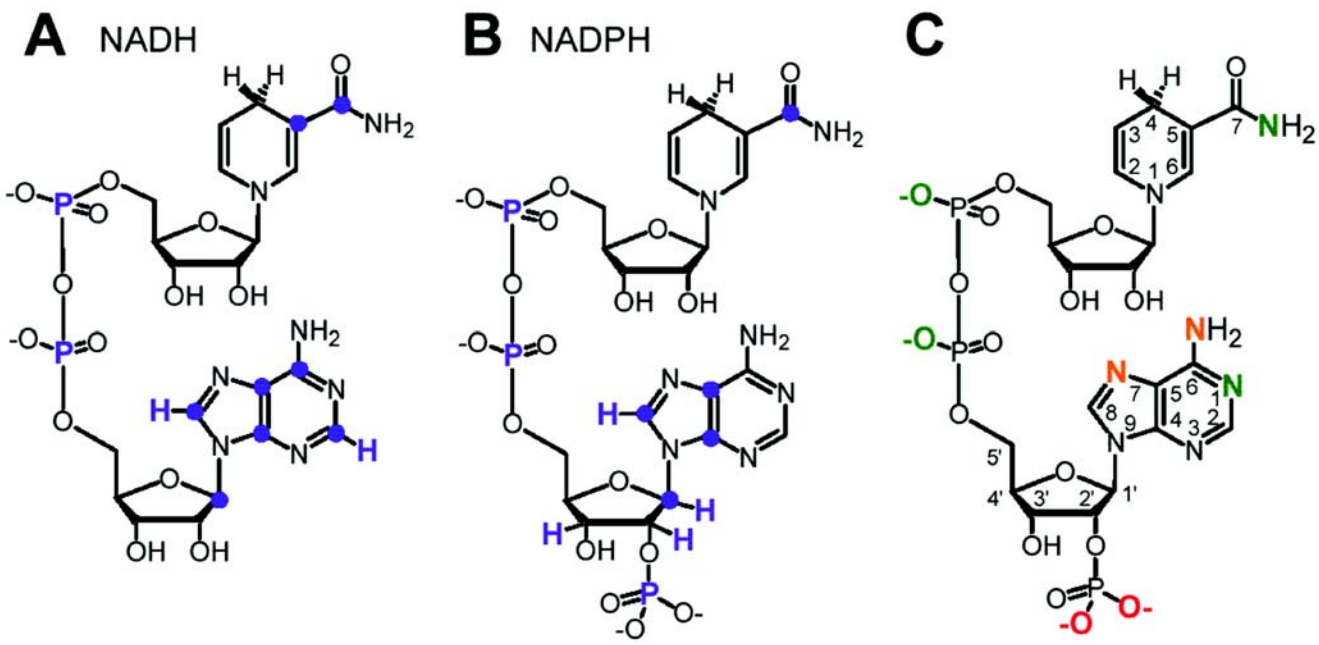

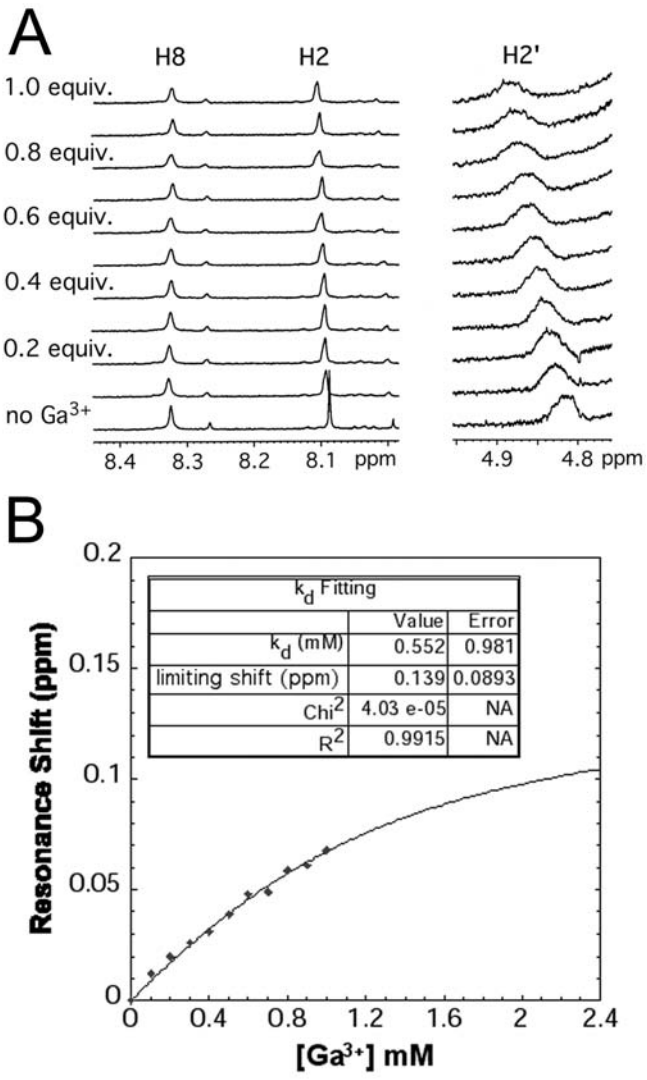

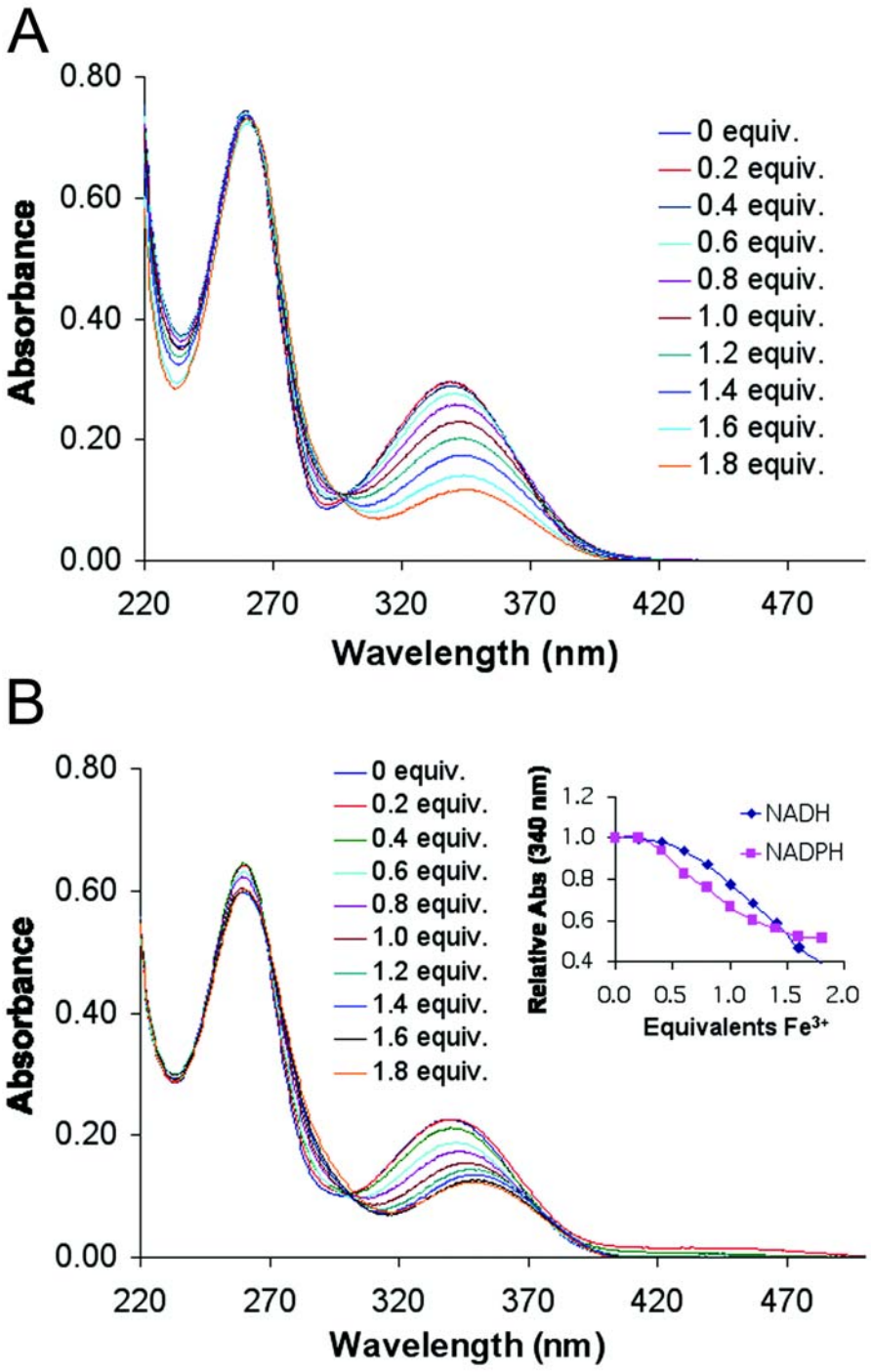

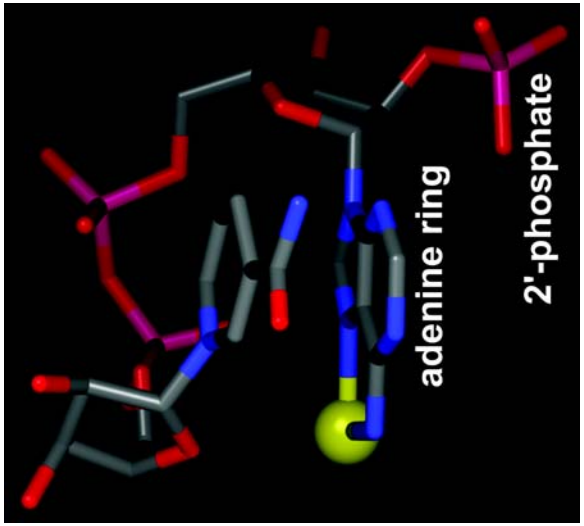

SUPPLEMENTARY TABLES AND FIGURE LEGENDS

TABLE S1. *Ga^{3+}-Induced Shifting of NADPH NMR resonances.*

For ^{1}H and ^{31}P NMR experiments, the concentration of NAD(P)H was 1 mM in D_2O with 2.0 equivalents of Ga^{3+} ($P_{2'}$, 2'-phosphate; P_{py}, backbone pyrophosphate). For ^{31}P NMR experiments, the concentration of NADPH was 10 mM in D_2O with 1.0 equivalent of Ga^{3+}. For ^{13}C NMR experiments, the concentration of NAD(P)H was 100 mM in D_2O with 0.4 equivalents of Ga^{3+}. Negative shifts in Hz are upfield.

$^{1}H/^{31}P$ NMR		Resonance shifting (Hz)
	Resonance	NADPH
Adenine	H2	55.0
	H8	88.0
	H1'	48.0
	H2'	100.0
	H3'	36.0
	H4'	24.0
	$H5'_R$	5.0
	$H5'_S$	0.0
Nicotinamide	H2	17.5
	$H4_R$	22.0
	$H4_S$	5.0
	H5	a
	H6	20.0
	H1'	a
	H2'	a
	H3'	0.0
	H4'	25.0
	$H5'_R$	18.0
	$H5'_S$	18.0
Phosphates	$P_{2'}$	-788
	P_{py}	-18.2
^{13}C NMR		Resonance shifting (Hz)
	Resonance	NADPH
Adenine	C2	-39.0
	C4	-10.0
	C5	-14.0
	C6	-33.0
	C8	-31.0
	C1'	-28.0
	C2'	-28.0
	C3'	-7.0
	C4'	-30.0
	C5'	-3.0
Nicotinamide	C2	2.1
	C3	-0.3
	C4	-1.0
	C5	2.4
	C6	1.5
	C7	-1.0

C1’	0.6
C2’	1.1
C3’	1.6
C4’	-3.8
C5’	-0.0

[a] Resonance overlaps D_2O signal or other resonances.

TABLE S2. *Ga^{3+}-Induced shifting of NMNH NMR resonances.*

For the ^{1}H and ^{31}P NMR experiments, the concentrations were 10 mM NMNH in D_2O, with 0.4 equivalents of Ga^{3+} (P_t, terminal phosphate). For the ^{13}C NMR experiments, the concentrations were 50 mM NMNH in D_2O, with 0.4 equivalents of Ga^{3+}. Negative shifts in Hz are upfield.

$^{1}H/^{31}P$ NMR	Resonance	Resonance shifting (Hz)
Nicotinamide	H2	-1.5
	$H4_R$	2.0
	$H4_S$	2.0
	H5	0.0
	H6	-10.5
	H1'	6.5
	H2'	-17.0
	H3'	-3.0
	H4'	10.5
	$H5'_R$	40.0
	$H5'_S$	40.0
Phosphate	P_t	-444
^{13}C NMR	Resonance	Resonance shifting (Hz)
Nicotinamide	C2	-4.7
	C3	7.2
	C4	0.0
	C5	2.2
	C6	-7.7
	C7	0.0
	C1'	3.0
	C2'	-6.7
	C3'	6.0
	C4'	-32.0
	C5'	60.0

FIG. S1. **HPLC column profiles of nicotinamide nucleotides.** Extracts and profiles were obtained as described in Experimental Procedures. The upper panel is a profile of a mixture of 3 nmol of each of the standards, whereas the lower panels are profiles of extracts from *E. coli* treated with the indicated concentrations of H_2O_2 as described in Experimental Procedures.

FIG. S2. **Absorbance spectra of NADPH with Ga^{3+}.** $Ga(NO_3)_3$ was added to 66 μM NADPH as indicated before recording the spectra.

FIG. S3. **Absorbance spectra of the charge transfer band of NADH and NADPH with Fe^{3+}.** 0.4 Equivalents of Fe^{3+} as $Fe(NO_3)_3$ was added to 500 μM NAD(P)H before recording the

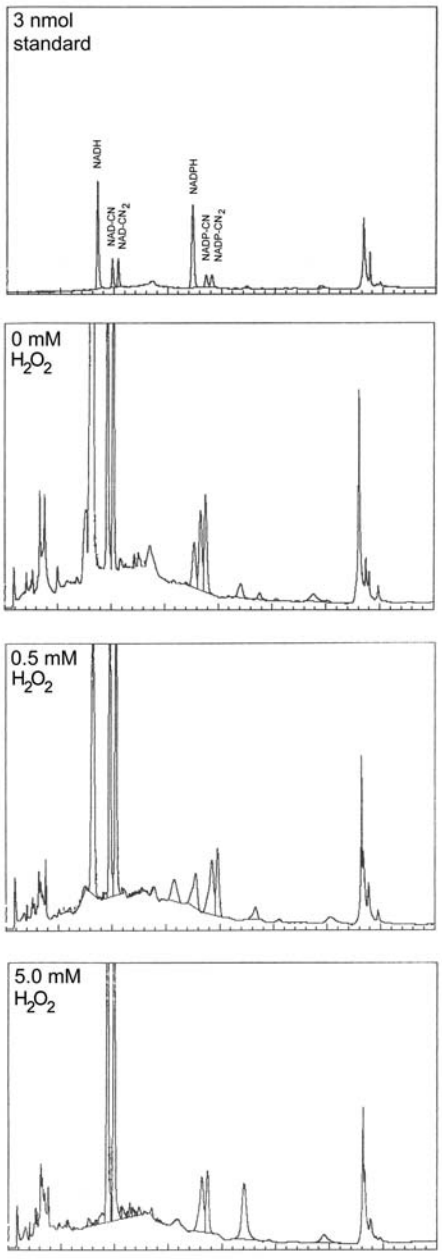

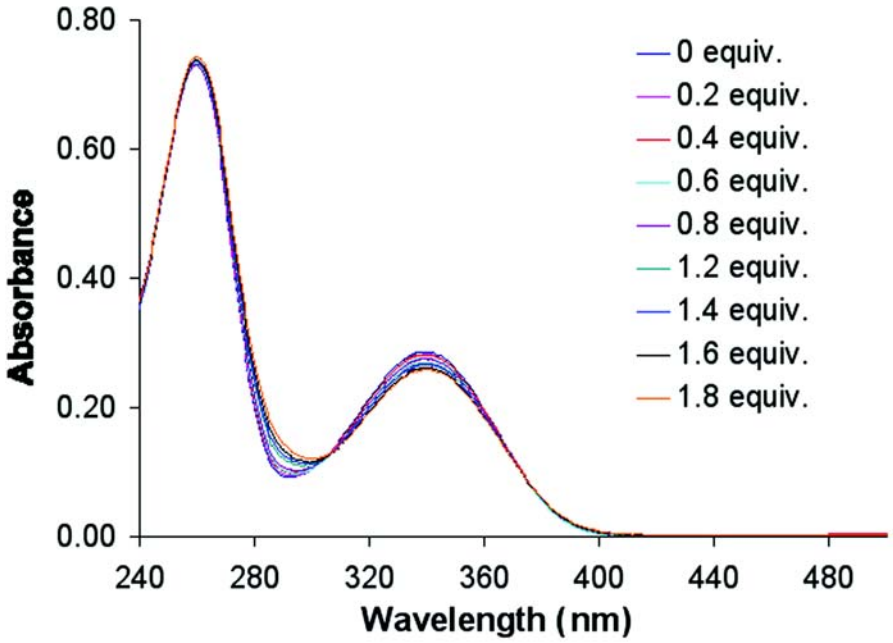

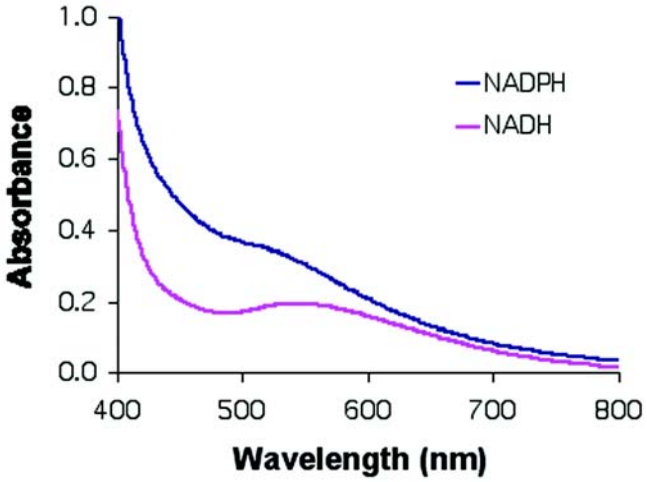

Effects of hydrogen peroxide upon nicotinamide nucleotide metabolism in Escherichia coli: Changes in enzyme levels and nicotinamide nucleotide pools and studies of the oxidation of NAD(P)H by Fe(III)

Julia L Brumaghim, Ying Li, Ernst Henle and Stuart Linn

J. Biol. Chem. published online August 11, 2003
